10. Vincent, J. M., Distortion of fungal hyphae in the presence of certain inhibitors. *Nature*, 1947, **150**, 850.
11. Glick, B. R., The enhancement of plant growth by free living bacteria. *Can. J. Microbiol.*, 1995, **41**, 109–117.
12. Gomez, K. A. and Gomez, A., *Statistical Procedure for Agricultural Research*, John Wiley and Sons, New York, 1976, 2nd edn, pp. 357–427.
13. Daimon, H., Nobuta, K., Ohe, M., Harada, J. and Nakayama, Y., Tricalcium phosphate solubilization by root nodule bacteria of *Sesbania cannabina* and *Crotalaria juncea. Plan Prod. Sci.*, 2006, **9**, 388–389.
14. Vazquez, P., Holguin, G., Purenti, M. E., Lopez-Cortes, A. and Bashan, Y., Phosphate-solubilizing microorganisms associated with the rhizosphere of mangroves in a semi-arid coastal lagoon. *Biol. Fert. Soil*., 2000, **30**, 460–468.
15. Jeon, J. S., Lee, S. S., Kim, H. Y., Ahn, T. S. and Song, H. G., Plant growth promotion in soil by some inoculated microorganisms. *J. Microbiol.*, 2003, **41**, 271–276.
16. Relwani, L., Krishna, P. and Reddy, M. S., Effect of carbon and nitrogen sources on phosphate solubilization by a wild-type strain and UV-induced mutants of *Aspergillus tubingensis*. *Curr. Microbiol*., 2008, **57**, 401–406.
17. Glick, B. R., Panrose, D. M. and Li, J., A model for the lowering of plant ethylene concentration by plant growth promoting rhizobacterium *Pseudomonas putida* GR 12-2. *Soil Biol. Biochem.*, 1998, **29**, 1233–1239.
18. Ahmad, F., Ahmad, I. and Khan, M. S., Indole acetic acid production by the indigenous isolates of *Azotobacter* and fluorescent *Pseudomonas* in the presence and absence of tryptophan. *Turk. J. Biol*., 2005, **29**, 29–34.
19. Sultana, S., Sharma, N. and Shirkot, C. K., Production of antifungal antibiotic by a newly isolated strain of *Bacillus megaterium. J. Microbial. World*, 2004, **6**, 8–15.
20. Ramirez, A. R., Abarca, E., Aquilar, U. G., Hayward-Jones, P. M. and Barboza, J. E., Antifungal activity of *Bacillus thuringiensis* chitinase and its potential for the biocontrol of phytopathogenic fungi in soybean seeds. *J. Food Sci.*, 2004, **69**, M131–M134.
21. Cazorla, F. M., Romero, D., Garcia, A. P., Lugtenberg, B. J. J., Vincente, A. and Bloemberg, G., Isolation and characterization of antagonistic *B. subtilis* strains from the avocado rhizoplane displaying biocontrol activity. *J. Appl. Microbiol.*, 2007, **103**, 1950–1959.
22. Buysens, S., Heungens, K., Poppe, J. and Hofte, M., Involvement of pyochelin and pyoverdin in suppression of pythium-induced damping off of tomato by *Pseudomonas aeruginosa* TNSKZ. *Appl. Environ. Microbiol.*, 1996, **62**, 865–871.
23. Srivastav, S., Yadav, K. S. and Kundu, B. S., Prospects of using phosphate solubilizing *Pseudomonas* as biofungicide. *Indian J. Microbiol.*, 2004, **44**, 91–94.
24. Shirkot, C. K. and Vohra, I., Characterization of novel carbendazim tolerant *Bacillus subtilis* with multiple plant growth promoting activities. Proceedings of XVI International Plant Protection Congress, BCPC, SECC, Glassgow, Scotland, UK, 2007, vol. 1, pp. 272–277.
25. Hwangbo, H. *et al.*, 2-ketogluconic acid production and phosphate solubilization by *Enterobacter intermedium. Curr. Microbiol*., 2003, **47**, 87–92.
26. Ivanova, R., Bojnova, D. and Nedialkova, K., Rock phosphate solubilization by soil bacteria. *J. Uni. Chem. Tech. Met.*, 2006, **41**, 297–302.
27. Ehrlich, H. L., Microbiologische und biochemische verfahrenstechnik. *Geomicrobiology*, Dekker, New York, 1990, pp. 120–140.
28. Alam, S., Khalil, S., Ayub, N. and Rashid, M., *In vitro* solubilization of inorganic phosphate by phosphate solubilizing microorganisms (PSM) from maize rhizosphere. *Int. J. Agric. Biol.*, 2002, **4**, 454–458.
29. Kumar, V. and Narula, N., Solubilization of inorganic phosphates and growth emergence of wheat as affected by *Azotobacter chroococcum* mutants. *Biol. Fert. Soil.*, 1999, **28**, 301–305.
30. Dave, A., and Patel, H. H., Inorganic phosphate solubilizing soil pseudomonads. *Indian J. Microbiol*., 1999, **39**, 161–164.
31. Goenadi, D. H., Siswanto and Sugiarto, Y., Bioactivation of poorly soluble phosphate rocks with a phosphorus-solubilizing fungus. *Soil Sci. Soc. Am. J.*, 2000, **64**, 927–932.

ACKNOWLEDGEMENT. We thank the ICAR (AINP on Biofertilizer), New Delhi, India for financial assistance.

Received 24 February 2009; revised accepted 11 January 2010

Using fallout ^{210}Pb measurements to estimate sedimentation rate in Lam Phra Phloeng dam, Thailand

Sasimonton Moungsrijun[1,*], Kanitha Srisuksawad[2], Kosit Lorsiririrat[3] and Tuangrak Nantawisarakul[1]

[1]Department of Physics, Faculty of Science, King Mongkut's University of Technology, Thonburi, Bangkok 10140, Thailand
[2]Nuclear Research and Development Group, Thailand Institute of Nuclear Technology, 16 Vibhavadi-Rangsit Road, Bangkok 10900, Thailand
[3]Office of Hydrology and Water Management, Royal Irrigation Department, 811 Samsean Road, Bangkok 10300, Thailand

The Lam Phra Phloeng dam was constructed in 1963 and is located in the Nakhon Ratchasima province. The dam has severely reduced water level caused by deforestation and agriculture at the upper land. Sediment cores were collected using a gravity corer. The ^{210}Pb activities were measured using alpha and gamma spectrometry and sedimentation rates were determined. The sedimentation rates decreased gradually from the upstream to the crest of the dam. The high sedimentation rate may be due to the inflow from the tributary as well as eroded materials that come from the upland area to the dam.

Keywords: Lam Phra Phloeng dam, ^{210}Pb, sedimentation rate.

SEDIMENTATION and siltation in water supply dams are widespread problems affecting the viability of the water supply systems. The siltation results from settlement of sediments carried by rivers and causes a number of pro-

*For correspondence. (e-mail: sasiphy@hotmail.com)

blems such as rapid reduction of the ability to store the maximum quantity of water; promotion of weed growth on the increased area of shallow margins which might affect water quality; potential destabilization of the dam structure, and problems with water intake and distribution systems, and higher frequency of unacceptable turbidity of water.

The Lam Phra Phloeng dam, located in the Nakhon Ratchasima province, is one of the dams most severely affected by sediment accumulation in Thailand. During the past 10 years, deforestation in the upper catchments has reduced the forest area by 70% from 531 km^2 in 1974 to 160.25 km^2 in 1985. Land use in the area changed rapidly from forest to agricultural land. The dominant crops are sugarcane and cassava. The land is tilled after harvesting and has become sensitive to sheet erosion. The area suffers periodically from floods and droughts. Increased erosion since forest clearance has led to the increase of sediment load in rivers draining into the reservoir. As a result, sediment deposition in the dam gradually decreased the water storage capacity from 150 million m^3 in 1970 to 121 and 108 million m^3 in 1983 and 1991 respectively[1]. The suspended sediments in the water bodies also affect water quality and cause pollution because of various agrochemicals adsorbed by the sediments into the catchments.

All these natural and human manipulations have accelerated the change of sedimentation rate in the dam. A refined method is needed to describe processes of sediment accumulation. Artificial and natural radioisotopes like ^{137}Cs and ^{210}Pb were known to provide useful information as tracers, which generate reasonable age estimates for sediments and the determination of the sediment accumulation rates[2].

^{137}Cs interacts strongly with micaceous clay minerals in soils and sediments[3]. ^{137}Cs (half-life 30.2 yr) is produced by nuclear fission and has been released into the environment as a result of nuclear weapon testing during 1950–70, maximum atmospheric inputs in 1963, and the Chernobyl accident in 1986. However, nuclear weapon-derived ^{137}Cs inputs were shown to be significantly lower in the southern hemisphere than in the northern hemisphere[4]; also inputs in the equatorial areas were less than those in the mid-latitude areas of Europe and North America[5]. The low ^{137}Cs inventories associated with these areas of reduced receipt of fallout introduce measurement problems in terms of both detection limits and the long count times required to obtain results with an acceptable degree of precision. ^{210}Pb (half-life 22.26 yr) is continuously deposited on to soil and sediment surface. ^{210}Pb is a natural product of the ^{238}U decay series and is derived from the decay of gaseous ^{222}Rn, the daughter of ^{226}Ra. ^{226}Ra occurs naturally in soils and rocks and will generate ^{210}Pb which will be in equilibrium with its parent[6]. On the other hand, ^{222}Rn gas produced from the decay of ^{226}Ra can diffuse and produce ^{210}Pb into the atmosphere. As fallout radionuclide ^{210}Pb is rapidly and strongly adsorbed to the surface soil and is horizontally redistributed within sediments, it has no effect on core chronology[7].

The total ^{210}Pb that is present in the sediment has two components: first a minor part in equilibrium with ^{226}Ra fixed to the sediment from ^{238}U decay and secondly, ^{210}Pb has a major part that is adsorbed on to the particulate matter, known as unsupported ^{210}Pb. It is formed in the atmosphere after ^{222}Rn decay and is deposited on the surface with the particle materials. The exponential decrease of the accumulated unsupported ^{210}Pb can be used to estimate sediment accumulation rate[8]. The required measurements of ^{210}Pb and ^{226}Ra activity can be made conveniently by direct gamma spectrometry using low-energy, low background HPGe detector or by alpha spectrometry via its daughter ^{210}Po.

The aim of this study is to estimate the sediment accumulation rate in Lam Phra Phloeng dam by the application of ^{210}Pb measurements using the construction of the dam in 1963 as a reference. Such data are required for assessment of the magnitude of the problems and for better understanding of the factors involved. Soil conservation measures and policies will hopefully be framed based on scientific knowledge.

The Lam Phra Phloeng dam located in Nakhon Ratchasima province in the northeastern region of Thailand (Figure 1) was constructed in 1963 and became operational four years later. It is located in the upper part of Lam Phra Phloeng river in a small catchment area of 820 km^2 between 14°30′–14°36′N and 101°47′–101°50′E. The average annual inflow along this river is 241.93 million m^3. The asterisk in Figure 1 indicates the crest of the dam. The reservoir length is about 11 km and has a depth of 15–25 m. The retention of the dam is 263 above mean sea level (msl) and the dead storage is 240 above msl. The ecology along the east and the west sides of the dam is still a natural forest.

Sediment cores were collected in September 2006 using a gravity corer. Transparent PVC core tubes (diameter of

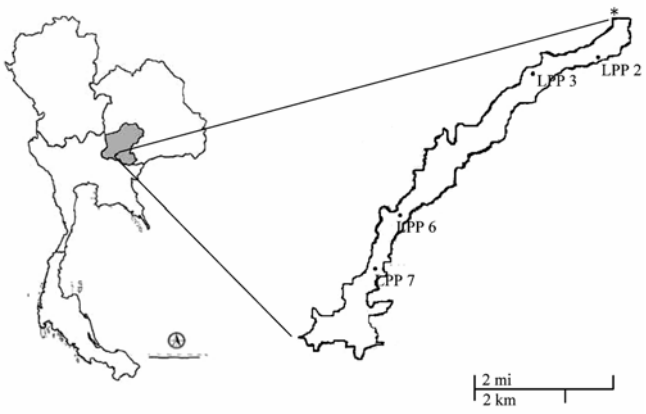

Figure 1. Map of Lam Phra Phloeng dam showing sample location.

5.4 cm and length of 75 cm) were inserted into the sediment. Sediment cores were then sliced into segments of 1 cm thickness by extrusion immediately and stored in a plastic bag. The outer part of each section was removed to avoid contamination from contiguous sections during the coring operation. The sediment was frozen at 4°C and transported in an ice box. In the laboratory, each slice was divided into subsamples to determine particle size, organic matter content and radioactivity. For particle size determination, the sample was stored in a refrigerator at 4°C until determination. The rest of the sample was weighed and dried at 60°C until the sediment weight was constant. The sediment was pulverized in a centrifugal ball mill and sieved through a 125 μm stainless steel sieve to achieve uniform particle size.

Organic matter content was determined by weight loss after 4 h ignition at 550°C (ref. 9). Pore water content was determined by weight loss after oven drying. Dry solid particle density was measured by Ultrapycnometer 1000 and ranged from 2.96 to 3.02 g cm^{-3}.

Determination of ^{210}Pb (via ^{210}Po) was performed on 3 g of dried sediment. After adding ^{209}Po standard tracer, the sediment was digested by sequentially adding concentrated HNO_3, $HClO_4$ and HCl[10]. The Po isotopes were then autoplated on to a silver disc suspended in mild HCl solution. Adding ascorbic acid prevented oxidation of Fe and its deposition on the silver disc. Po activity was measured on an alpha spectrometry system (Ortec ion-implanted, silicon, partially depleted, charged-particle detectors coupled to Tennelec multichannel analysers). Radioisotopes (^{241}Am, ^{244}Cu and ^{239}Pu) were used for energy and efficiency calibration.

^{226}Ra activity was determined by gamma spectrometry. The sample was placed in a sample ampoule of a diameter of 10 and 30 mm height, weighed and sealed. The sample spectrum was measured after waiting for at least 3 weeks to allow ingrowths of ^{222}Rn progeny. The peak counts integrated at 351.9 and 609.3 keV of ^{214}Pb and ^{214}Bi respectively[11]. The gamma-ray spectrometry system was a GWL series HPGe (high-purity germanium) coaxial well with 0.5 mm aluminum absorbing layers (well wall) thickness, mounted in a vacuum tight cryostat (Model GWL-120230, crystal diameter 54.9 mm, well inside diameter 10 mm and active well depth 40 mm), a liquid-nitrogen Dewar and dipstick cryostat (Model HJ-GWL) and 1500 volts high voltage supply. A computer-based MCA (DSPEC) and GammaVision-32 V 3.2 Gamma-Ray Spectroscopy Software, a graphical user interface, that is ideal for manipulation and analysis of spectra with a personal computer was used. Radioisotopes (^{133}Ba, ^{152}Eu, ^{137}Cs and ^{60}Co) were used for energy and efficiency calibrations.

Total ^{210}Pb activity was determined indirectly by the measurement of its alpha emitting grand daughter nuclide ^{210}Po. The total ^{210}Pb activities are a ratio of ^{210}Po and ^{209}Po counts. Subtracting of supported ^{210}Pb from total ^{210}Pb can determine unsupported ^{210}Pb. The activity of total ^{210}Pb is obtained by the formula[12]:

$$A(^{210}\mathrm{Pb}) = \left(\frac{N_{210}(\mathrm{s}^{-1})}{N_{209}(\mathrm{s}^{-1})}\right)\left(\frac{A(^{209}\mathrm{Po})}{\text{sediment weight (g)}}\right), \qquad (1)$$

where N_{210} and N_{209} are the alpha counts of the polonium isotope; A(^{210}Pb) the total ^{210}Pb activities; A(^{209}Po) the decay ^{209}Po decay activity coefficient (24.575 dpm ml^{-1}).

And finally, determination of ^{210}Pb chronologies and sedimentation rate was performed using the constant initial concentration (CIC) model. This was originally developed by Goldberg in 1963, although its first application to lake sediments was by Krishnaswamy *et al.*[13]. The CIC model assumes that, each stage of sediment accumulation, has a constant initial unsupported ^{210}Pb concentration.

$$A = A_0\, e^{-\lambda t} = A_0\, e^{-\lambda(m/w)}, \qquad (2)$$

where A_0 is the ^{210}Pb activity at water–sediment interface (Bq kg^{-1}); A the ^{210}Pb activity in the sediment (Bq kg^{-1}); λ the decay constant of ^{210}Pb (0.03114 yr^{-1}); m the cumulative dry mass (g cm^{-2}); w the sedimentation rate (g cm^{-2} y^{-1}).

Profiles of ^{210}Pb obtained from cores collected in the reservoir were used to calculate apparent sedimentation rates by assuming the steady-state deposition of ^{210}Pb. Sediment activities are reported as functions of cumulative dry mass per unit area (g cm^{-2}) to eliminate the effect of porosity and dry bulk density changes with depth. The sedimentation rates were determined from the expression $w = -\lambda/b$, where b can be determined by the slope of the least squares fit to the natural log (unsupported ^{210}Pb) versus cumulative dry mass curve, however in the figure, the unsupported ^{210}Pb is shown in numerical value.

Organic matter content of dry sediment samples ranged from 8% to 14% with an average of 11%. This result could be explained as a regular trend of organic matter in

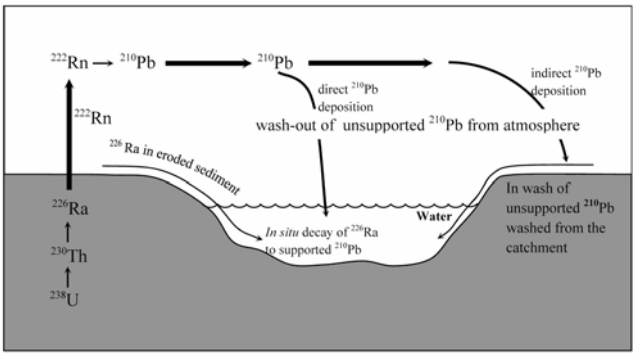

Figure 2. Pathways by which ^{210}Pb reaches sediments in lakes and reservoirs.

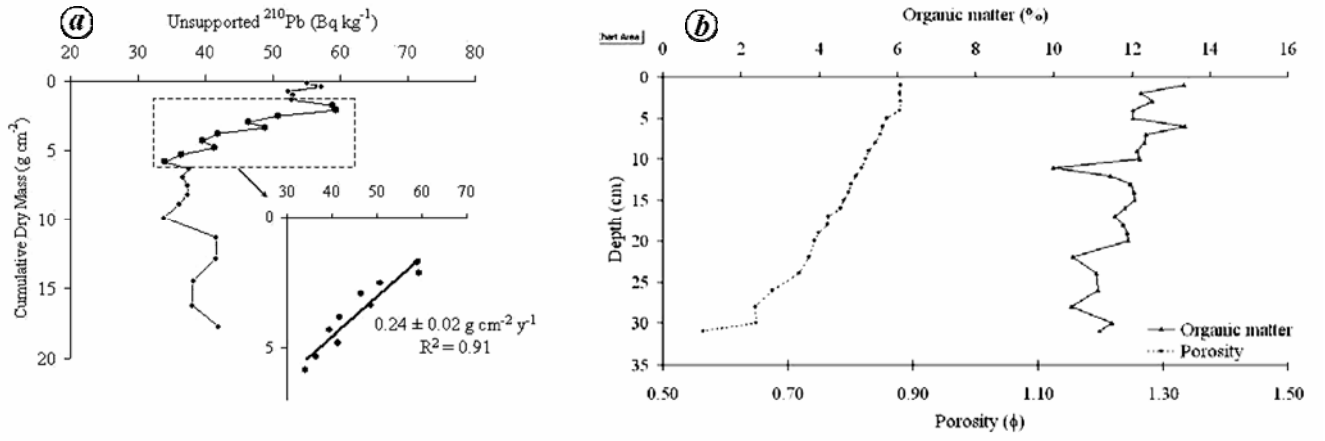

Figure 3. LPP2: ***a***, Linear unsupported ^{210}Pb; ***b***, Porosity and organic matter.

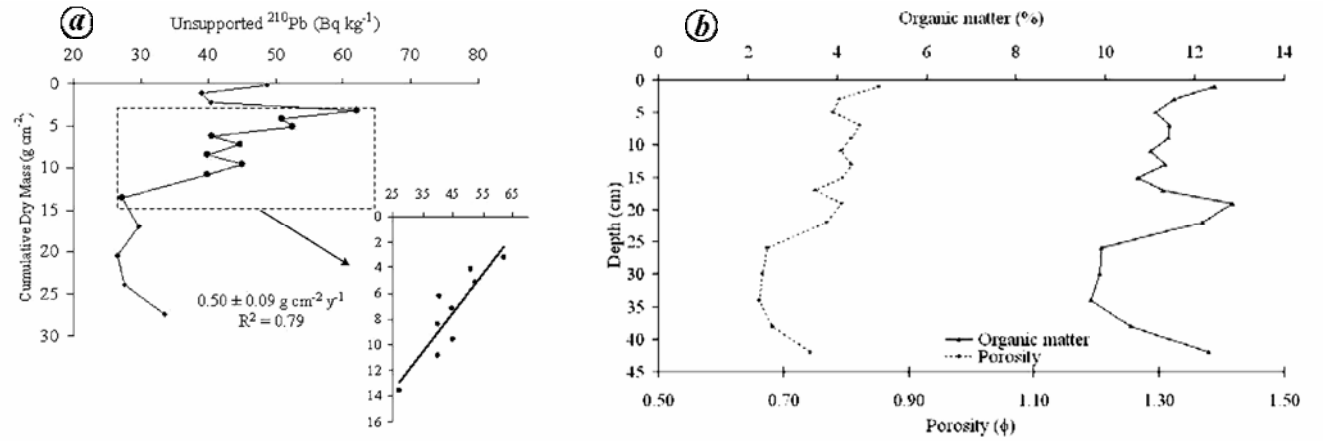

Figure 4. LPP3: ***a***, Linear unsupported ^{210}Pb; ***b***, Porosity and organic matter.

the agricultural lands where the farmers plant their crops every year.

In this study, the porosity of the sediments was determined, which is closely related to water content of the sediments and in addition depends on the density of solid matter[14]. The sediment compaction has great impact on the porous surfaces where there is high water content and low bulk density. Normalizing core section widths to that of the deeper regions where there is low water content and high bulk density can decrease section width of the upper region and decrease the apparent penetration of lead radionuclides. The porosity of sediments is usually high (>0.80) near the water–sediment interface. However, deep down it decreases and lowers the rate constant and changes in a narrow internal.

Sedimentation rates in each region of the dam as shown in Figure 2 were determined using vertical distributions of unsupported ^{210}Pb in sediment cores. Actually, eight sediment cores were collected for this study. However after ^{210}Pb analysis, only four (LPP2, 3, 6 and 7) were successfully analysed for sedimentation rates. The other four did not show ^{210}Pb activity decrease with depth and therefore did not fit the model. The estimation of sedimentation rates is described here (Figures 3–6).

The ^{210}Pb activities at the surface of the cores LPP2, 3, 6 and 7 did not decrease with depth and showed mixing behaviour due to biological or physical processes or both. The mixing layer could be observed from the surface till 5, 7, 14 and 4 cm depth of the cores LPP2, 3, 6, and 7 respectively. Under these depths, the ^{210}Pb activity showed decrease with depth and could be used for sedimentation rate estimation. Many other cores from shallow water stations exhibit nonlinear behaviour deep down in the cores and cannot be used for sedimentation rate estimation.

Figure 3 shows ^{210}Pb profile of LPP2. For LPP2, sediment core length is 31 cm. The irregular profile of ^{210}Pb activity was from the surface to 5 cm. The sedimentation rates estimated from ^{210}Pb profile from the depth of 5–15 cm were 0.24 ± 0.02 g cm^{-2} yr^{-1}. Unsupported ^{210}Pb activity ranged from 33.83 to 59.29 Bq kg^{-1} and the porosity ranged from 0.62 to 0.90. Supported ^{210}Pb activity derived from activity at depth was 9.10 Bq kg^{-1}. Table 1 summarizes the core location, sediment properties and

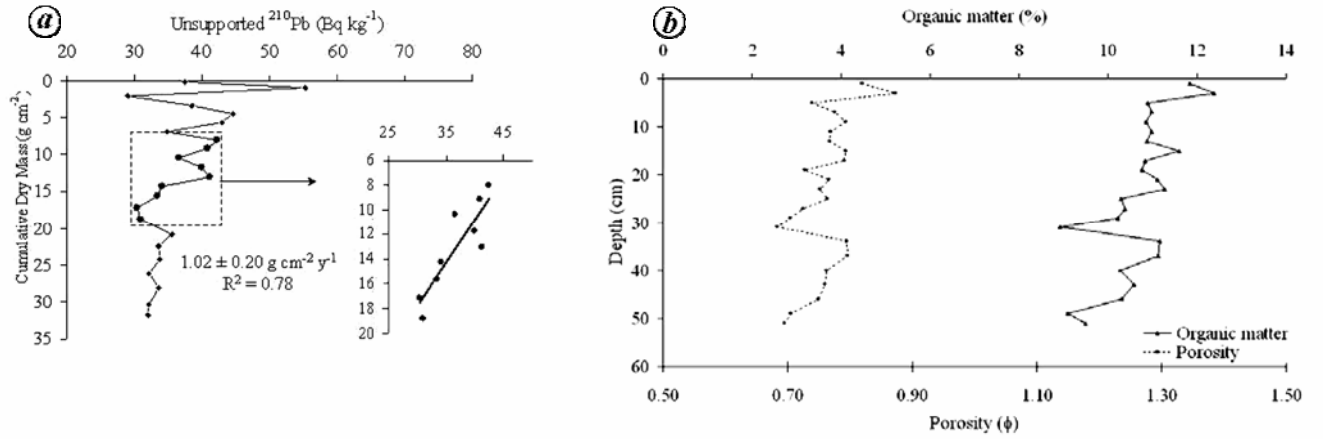

Figure 5. LPP6: ***a***, Linear unsupported ^{210}Pb; ***b***, Porosity and organic matter.

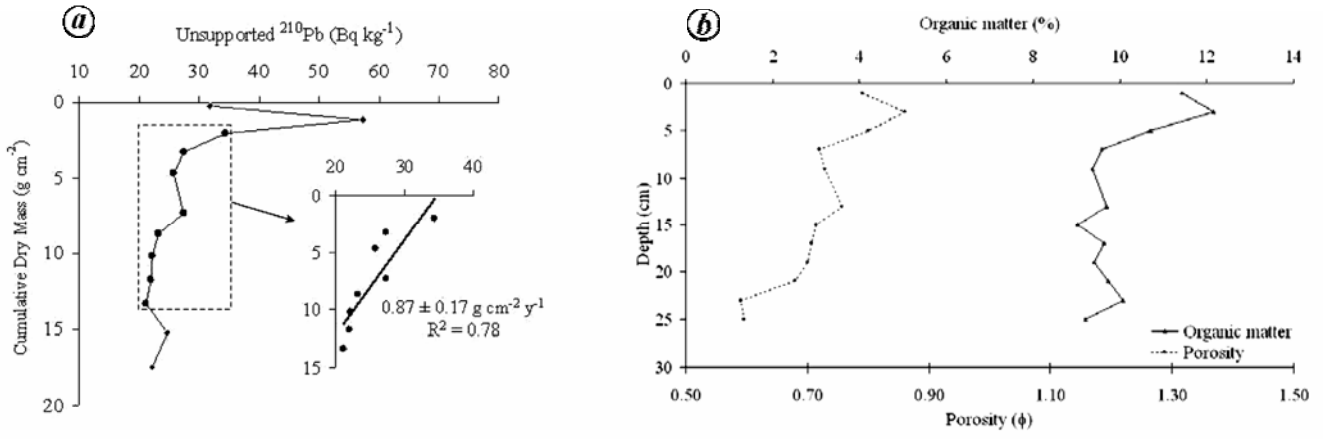

Figure 6. LPP7: ***a***, Linear unsupported ^{210}Pb; ***b***, Porosity and organic matter.

Table 1. Core location, sediment properties and sedimentation rates of cores LPP2, 3, 6 and 7

	Site of core			
Description	LPP2	LPP3	LPP6	LPP7
Location (UTM)	805720 E 1615002 N	804651 E 1614465 N	802303 E 1612011 N	801151 E 1609948 N
Core range (cm)	31	43	51	26
Porosity	0.62–0.90	0.70–0.90	0.71–0.89	0.64–0.89
Surface mixed layer, SML (cm)	0–5	0–7	0–14	0–4
Unsupported ^{210}Pb activity (Bq kg^{-1})	33.83 ± 7.97 to 59.29 ± 13.35	26.64 ± 6.34 to 61.98 ± 12.81	28.92 ± 7.34 to 55.27 ± 11.90	21.15 ± 5.11 to 57.15 ± 11.96
Supported ^{210}Pb activity (Bq kg^{-1})	9.10 ± 1.38	5.05 ± 0.67	8.04 ± 1.05	7.01 ± 0.95
Sedimentation rate (g cm^{-2} yr^{-1})	0.24 ± 0.02	0.50 ± 0.09	1.02 ± 0.20	0.87 ± 0.17

sedimentation rates of cores LPP2, 3, 6 and 7 which relate to Figures 3–6.

As shown in Table 1, the relation between the cores is revealed in parameters such as porosity, surface mixed layer and sedimentation rate. The porosity of all cores is similar (range 0.60–0.90). The surface mixed layer of cores is also similar except that of LPP6 which is deeper than those of the other cores, i.e. 14 cm in LPP6 compared to 4–7 cm in other cores. The depth of the surface mixed layer of the cores depends on the water in-flow velocity, gravitational forces and other factors such as bottom slope. Clearly, support was from the high sedimentation rate at LPP6; 1.02 ± 0.20 g cm^{-2} yr^{-1} which received sediment from the tributary inflow and eroded

materials from upland areas adjacent to the dam. Sedimentation rate was continually increased with distance from the crest of the dam to the upstream.

It is clear from Figures 3–6 that total ^{210}Pb activity was variable in each core. This is because the ^{210}Pb deposited on land can be transported to nearby water resources adding to the ^{210}Pb already present in water. Also natural, unsupported ^{210}Pb in the atmosphere can be deposited everywhere; it may accumulate on land or in water. ^{210}Pb activity in water is increased in the area near the end of upstream portion of the dam. As a result, the colour of the sediment upstream is red brick with coarse particles, whereas the downstream sediments are dark in colour and fine particles.

This communication demonstrates the application of ^{210}Pb activity in characterizing the important factors affecting sediment characteristics of Lam Phra Phloeng dam. The radioactivities, ^{210}Pb and ^{226}Ra were determined by alpha and gamma spectrometry. From the analysis, the sedimentation rate and its relationship in each part of the dam is established. The sedimentation rate estimated ranges from 0.24 to 1.02 g cm^{-2} y^{-1} and shows an increase from the crest of the dam to the upstream area.

1. Lorsirirat, K., *Effect of Forest Cover Change on Sedimentation in Lam Phra Phloeng Reservoir, Northeastern Thailand*, Springer, Japan, Shinano Inc, Japan, 2007.
2. Walling, D. E., Using environmental radionuclides to trace sediment mobilisation and delivery in river basins as an aid to catchment management. Proceedings of the Ninth International Symposium on River Sedimentation, Yichang, China, 18–21 October 2004.
3. Comans, R. N. J., Middelburg, J. J., Zonderhuis, J., Woittiez, J. R. W., De Lange, G. J., Das, H. A. and Van Der Weijden, C. H., Mobilization of radiocaesium in pore water of lake sediments. *Nature*, 1989, **339**, 367–369.
4. Zhang, X. and Walling, D. E., Characterizing land surface erosion from cesium-137 profiles in lake and reservoir sediments. *J. Environ. Qual.*, 2005, **34**, 514–523.
5. Walling, D. E. and He, Q., Using fallout lead-210 measurements to estimate soil erosion on cultivated land. *Soil Sci. Soc. Am.*, 1999, **63**, 1404–1412.
6. Zapata, F. and Garcia-Agudo, E., Future prospects for the ^{137}Cs technique for estimating soil erosion and sedimentation rate. *Acta Geol. Hispanica*, 2000, **35**, 197–205.
7. Zapata, F., The use of environmental radionuclides as tracers in soil erosion and sedimentation investigations: recent advances and future developments. *Soil Till. Res.*, 2003, **69**, 3–13.
8. Robbins, J. A., Geochemical and geophysical applications of radioactive lead isotopes. In *Biogeochemistry of Lead* (ed. Nriago, J. P.), Elsevier, Amsterdam, 1978, pp. 285–393.
9. Armentano, T. V. and Woodwell, G. M., Sedimentation rates in a long island marsh determined by ^{210}Pb dating. *Limnol. Oceanogr.*, 1975, **20**, 452–456.
10. Carpenter, R., Bennett, J. T. and Peterson, M. L., ^{210}Pb activities in and fluxes to sediments of the Washington Continental Shelf and slope. *Geochim. Cosmochim. Acta*, 1981, **45**, 1155–1172.
11. El-Aydarous, A., Gamma radioactivity levels and their corresponding external exposure of some soil samples from Taif Governorate, Saudi Arabia. *Glob. J. Environ. Res.*, 2007, **1**, 49–53.
12. Pizzolato, W. N. and De Hon, R. A., Lead-210 derived sedimentation rates from a North Louisiana paper-mill effluent reservoir. *Clays Clay Min.*, 1995, **43**, 515–524.
13. Gale, S. J., Haworth, R. J. and Pisanu, P. C., The ^{210}Pb chronology of lake Holocene deposition in an Eastern Australian Lake Basin. *Quat. Sci. Rev.*, 1995, **14**, 395–408.
14. Mažeika, J. and Gudelis, A., Component-based and radioisotope signature of lacustrine sediments in Eastern Lithuania. *Geologia*, 2006, **54**, 49–60.

ACKNOWLEDGEMENTS. We thank the King Mongkut's University of Technology Thonburi, the Royal Irrigation Department, Ministry of Agriculture and the Thailand Institute of Nuclear Technology, Ministry of Science and Technology for providing facilities and instruments.

Received 13 April 2009; revised accepted 27 January 2010

Sapphirine-bearing Mg–Al xenolith in Proterozoic kimberlite from Dharwar craton, southern India

S. C. Patel[1,*], S. Ravi[2], Y. Anilkumar[1] and J. K. Pati[3]

[1]Department of Earth Sciences, Indian Institute of Technology, Powai, Mumbai 400 076, India
[2]Geological Survey of India, Bandlaguda Complex, Hyderabad 500 068, India
[3]Department of Earth and Planetary Sciences, University of Allahabad, Allahabad 211 002, India

A rare crustal xenolith of Mg–Al rock recovered from the P3 pipe of Wajrakarur Kimberlite Field in the Dharwar craton contains the minerals sapphirine, spinel and phlogopite. All the minerals have low iron contents with X_{Mg} values of 0.97 in phlogopite, 0.95–0.96 in sapphirine and 0.87 in spinel. The (MgO, FeO) : (Al_2O_3) : SiO_2 ratio in sapphirine is close to 7 : 9 : 3. Sapphirine–spinel geothermometry indicates that the rock has undergone peak metamorphism in the amphibolite–granulite transition facies. Although sapphirine-bearing Mg–Al rocks are known from the northern and southern parts of Dharwar craton, this is the first report of such rocks from the central part of the craton.

Keywords: Dharwar craton, kimberlite, Sapphirine, spinel, xenolith.

SAPPHIRINE-bearing Mg–Al metamorphic rocks have attracted the attention of many geologists for more than a century on account of the interesting and complex mine-

*For correspondence. (e-mail: scpatel@iitb.ac.in)